




# Identifying photochemical alterations of dissolved pyrogenic organic matter using fluorescence spectroscopy

Jessica K. Egan<sup>1,2</sup> · Diane M. McKnight<sup>1,2</sup>  · Maggie M. Bowman<sup>1,2</sup> · Michael D. SanClements<sup>2,3</sup> · Adrian C. Gallo<sup>4</sup> · Jeff A. Hatten<sup>4</sup> · Lauren M. Matosziuk<sup>1,2,3,4</sup>

Received: 14 July 2022 / Accepted: 16 November 2022 / Published online: 27 January 2023  
© The Author(s) 2023

## Abstract

Many streams originate in forested watersheds at risk of wildfires. Wildfires can introduce thermally altered organic compounds to terrestrial and aquatic systems. Understanding the degradation of leachates from these burned organic materials, referred to as dissolved pyrogenic organic material (PyDOM), is critical in determining water quality impacts in forested watersheds. This study used fluorescence spectroscopy to examine photochemical alterations of PyDOM generated by leaching organic matter burned at various temperatures. The PyDOM was exposed to natural sunlight for 25 days and the photochemical formation of hydrogen peroxide was monitored. PyDOM was characterized using ultraviolet–visible absorption, excitation–emission matrix (EEM) fluorescence spectroscopy, and fluorescence indices. Throughout the experiment, the emission intensity of the humic peak for all light-exposed leachates decreased while dark leachates exhibited no significant change in their fluorescence spectra. Additionally, hydrogen peroxide concentrations and UV absorbance decreased progressively over time, providing direct evidence that PyDOM concentrations can be significantly reduced by photodegradation. A characteristically low emission peak was observed in the EEMs of the fresh PyDOM, which could help in detecting fresh PyDOM. These results demonstrate that PyDOM derived from burned leachates is susceptible to photodegradation and that fluorescence measurements could be used as proxies for detecting PyDOM immediately post-wildfire.

**Keywords** Wildfire · Dissolved pyrogenic organic matter · Photolysis · Fluorescence

## Introduction

Wildfires can impact aquatic systems by introducing into the water column a heterogeneous spectrum of thermally altered organic compounds, known as pyrogenic organic matter (PyOM) (Bird et al. 2015; Dittmar et al. 2012; United States Geological Survey (USGS) 2018). Within the contiguous United States, 46% of surface water supplies originate on

forested lands (including both federal and non-federal) (N. Liu et al. 2022a, b). Many of these forested watersheds are vulnerable to wildfires which have been increasing in frequency and severity for decades (Abatzoglou and Williams 2016; Buechi et al. 2021; Harvey 2016). These forested streams play an important role in the production, transport, and quality of dissolved organic matter (DOM) and dissolved PyOM (PyDOM) (Bird et al. 2015; Creed et al. 2015; Freeman et al. 2007). PyDOM compounds are introduced into the environment through both direct (wildfire combustion) and indirect (soil degradation and microbial oxidation) pathways (Bostick et al. 2021; Hockaday et al. 2007). For water treatment plant operators, PyDOM poses an increased risk of carcinogenic and mutagenic byproducts from pyrogenic toxicants and the formation of toxic disinfection byproducts (Uzun et al. 2020; Wang et al. 2015).

PyOM encompasses a wide range of organic compounds whose composition depends on the formation temperature and source material (Bostick et al. 2018; Myers-Pigg et al. 2015; Roebuck et al. 2018; Schneider et al. 2010; Wagner

✉ Diane M. McKnight  
diane.mcknight@colorado.edu

<sup>1</sup> Department of Environmental Studies, University of Colorado, Boulder, CO 80309, USA

<sup>2</sup> Institute of Arctic and Alpine Research, University of Colorado, Boulder, CO 80309, USA

<sup>3</sup> National Ecological Observatory Network, Battelle, Boulder, CO 80301, USA

<sup>4</sup> Department of Forest Engineering, Resources, and Management, Oregon State University, Corvallis, OR 97333, USA

et al. 2018; Wozniak et al. 2020). Lower combustion temperatures produce more water soluble and labile PyDOM containing more oxygenated functional groups (Bostick et al. 2018, 2021). These lower temperature PyDOM compounds include low molecular weight (MW) organic acids, thermal degradation byproducts of cellulose, and are an important substrate for heterotrophic bacteria and a source of highly mobile soil organic matter (Matosziuk et al. 2020; Myers-Pigg et al. 2015; Wagner et al. 2018). As formation temperatures increase, PyOM compounds become less water-soluble resulting in low concentrations of increasingly more condensed PyDOM (Bostick et al. 2018; Myers-Pigg et al. 2017; Santín et al. 2017; Ward et al. 2014). These higher temperature PyDOM compounds are more aromatic and comprised of fewer oxygenated functional groups, resulting in higher MW aromatic and condensed aromatic compounds—including polycyclic aromatic hydrocarbons (PAHs) (Goranov et al. 2020; Santín et al. 2017). Compared to particulate PyOM, PyDOM contains more oxygenated functional groups and smaller aromatic cluster sizes; and when compared to normal humic substances, PyDOM has higher aromatic and carboxylic carbon content and less aliphatic carbon content (Liu et al. 2022a, b; Qu et al. 2016).

PyOM can contribute to the chromophoric, or light absorbing fraction of DOM (CDOM) of natural waters. Photolysis of DOM is an important process of carbon cycling and transport, because CDOM attenuates solar radiation throughout the water column (Hader et al. 2003). Wagner et al. (2015) examined linkages and sources of dissolved black carbon (a subset of and therefore referred to here as PyDOM) and found that overland flow can mobilize and remove surface PyDOM, serving as a source of more condensed PyDOM compounds, and subsurface flow could be more responsible for the addition of less condensed PyDOM compounds (Wagner et al. 2015). Additionally, these high MW PyDOM compounds were particularly photolabile (Fu et al. 2016; Wagner et al. 2018; Wagner and Jaffé 2015). Fu et al. (2016) and Ward et al. (2014) both examined the photochemical transformations of PyDOM, reporting that the majority of PyDOM underwent partial photooxidation rather than complete photomineralization. Wagner et al. (2018) summarized several processes for PyDOM alteration including photodegradation, biodegradation, sorption, and co-precipitation. In particular, photo-reactivity varies across the PyDOM spectrum with increased photosensitivity exhibited by larger condensed aromatic structures (Wagner et al. 2018).

Within DOM, the molecules with aromatic-C groups serve as the main light absorbing fraction that initiates and assists in both direct and indirect photochemical reactions, which can produce reactive radicals or intermediate species, partially oxidized compounds, low MW aliphatic compounds, or  $\text{CO}_2$  (Ward and Cory 2016). Hydrogen peroxide

( $\text{H}_2\text{O}_2$ ) is a photochemical byproduct of DOM photolysis, the detection of which can be used to confirm photolysis (Cooper et al. 1988; McKay and Rosario-Ortiz 2015; Scott et al. 2003). Many PAHs are susceptible to photolysis (Abra-jano et al. 2007; Cory et al. 2007). The number of aromatic rings present dictates photoreactivity, with fewer rings (e.g. naphthalene) being less photoreactive than condensed structures (e.g. pyrene) (Fasnacht and Blough 2002; Pagni and Sigman 1999). Solar radiation contributions to DOM photolysis are 50% UVA, 25% UVB, and 25% attributed to photosynthetically active radiation (PAR), within the visible (Hader et al. 2003). Understanding PyOM degradation mechanisms and pathways is critical in determining PyOM transport between source (wildfire production), intermediate zones (soils, streams, and atmosphere), and sinks (aquatic sediments). Given that wildfires typically occur in summer, photolysis should play an important role in the attenuation of both labile and refractory PyDOM entering source waters following a wildfire.

Fluorescence spectroscopy is a robust tool for characterizing DOM and examining photochemical changes (Gabor et al. 2014; Cory and McKnight 2005; Wagner and Jaffé 2015). Condensed PAHs are typical of burned OM and may be responsible for the distinctive fluorescence signatures observed. Information contained within an excitation-emission matrix (EEM) can be quantified using fluorescence indices, where numerical values represent a ratio of fluorescence intensity signals comparing various regions or points within the EEM (Gabor et al. 2014). Both EEMs and indices provide information about the origin and transformation of DOM. Additionally, fluorescence is becoming increasingly utilized by water treatment plant (WTP) operators given that the measurements can be made quickly and require only a small volume of filtered water (Baker 2001; Bedell et al. 2022).

This study contributes to the growing body of work showing that PyDOM is susceptible to photodegradation and that fluorescence spectroscopy can be a meaningful tool in detecting and analyzing wildfire signatures. The main objectives were to use fluorescence spectroscopy EEMs and indices to capture the compositional changes of (1) PyDOM along a wide temperature burn spectrum, and (2) photochemical transformations throughout a 25-day sunlight exposure period. Given the wide range of temperatures that occur within a watershed impacted by wildfire, we generated seven leachates that differed according to burn treatment and represented various portions of the PyDOM spectrum. Artificial PyDOM was produced by burning OM (leaves and topsoil) in a muffle furnace at 200, 300, 400, 550, and 700 °C. Additionally, a controlled outside burn sample was generated to act as a comparison sample for natural conditions and then there was an unburned control. The burned OM was then leached and exposed to sunlight for

up to 25 days. Throughout the experiment the production of  $H_2O_2$  and various fluorescence signatures were concurrently tracked. This research demonstrates that PyDOM can exhibit unique fluorescence characteristics driven by burn temperature, burned leachates are susceptible to photodegradation, and with increased exposure to solar radiation the fluorescence signatures can resemble more natural OM overtime. The findings of this study are relevant to downstream water treatment plant operators and natural resources managers in examining post-wildfire water quality.

## Methods

### Site description

In August 2018, samples of leaf litter and soils were collected from four areas around Great Smoky Mountain National Park (GRSMNP), Tennessee, USA, within the southern Appalachian Mountains. The sampling sites included Briar Branch, Bearwallow, the Twin Creeks Science Center and a residential area in Sevierville. At each site, fallen leaf litter and soil were collected under trees representative of the surroundings. The GRSMNP is densely vegetated with extensive leaf litter, and is characterized as submesic to mesic oak-hardwood forests, southern Appalachian cove hardwood, and montane alluvial forest (Matosziuk et al. 2020). Primary tree species include hickory (*Carya* sp.), oak (*Quercus* sp.), red maple (*Acer rubrum* L.), eastern white pine (*Pinus strobus* L.), American Beech (*Fagus grandifolia*), sassafras (*Sassafras albidum*), and black gum (*Nyssa sylvatica*). Additional plant species include Virginia creeper (*Parthenocissus quinquefolia*), mountain laurel (*Kalmia latifolia* L.), rhododendron (*Rhododendron* sp.), and poison ivy (*Toxicodendron radicans*) (Matosziuk et al. 2020; National Park Service (NPS) 2019). Fallen leaf litter and loose O-horizon soil (up to 2 cm) were collected and stored separately in large polyethylene plastic bags. The soil and leaves were air-dried for 48 h onsite. Upon returning to Boulder, CO, soils were freeze-dried and leaf litter samples were oven-dried at 60 °C for 48 h to ensure uniform drying (Blank et al. 1996; Hansen et al. 2016). After drying, the total weight accumulated was 4.38 kg of leaves and 1.22 kg of soil. To account for vegetation variability, samples were later homogenized during the leaching phase.

### Combustion and leaching of leaf litter and soil

Natural wildfire PyOM production can differ from PyOM produced by combustion in a muffle furnace under controlled and stable conditions due to several factors, including variable maximum temperatures (500–950 °C), exposure to atmospheric gasses (i.e.,  $N_2$  and  $O_2$ ), and short heating

durations of wildfires (Blank et al. 1994, 1996; Brown et al. 2006; Novotny et al. 2015; Santín et al. 2017). PyOM production from wildfires results in PyOM that is more heterogeneous with higher O/C and H/C ratios (Santín et al. 2017). For the laboratory burns, leaves and soils were burned separately in pre-weighed uncovered porcelain dishes for 15 min in a pre-heated muffle furnace. Then, the samples were transferred to a desiccator and weighed upon cooling. For the outside burns, temperature was logged using two thermocouple probes and a Gain Express 4 Channel K Type Thermometer. The maximum temperatures were between 300 and 475 °C and the burns lasted between 15 and 20 min. For statistical analyses that involved numerical temperature inputs, the drying temperature of 60 °C was used to represent the unburned samples and the average temperature of 388 °C was used to represent the outside samples.

Throughout the leaching and exposure steps, all bottles, carboys, water, and other eligible equipment were autoclaved to maintain a sterile environment. Each temperature treatment, the unburned control, and a solution blank were leached separately in 20 L Nalgene carboys (Supplementary Fig. 1). Carboys were filled with a 15 L solution of 0.001 M sodium bicarbonate ( $NaHCO_3$ ) and 0.04% formaldehyde ( $CH_2O$ ) and then 225 g of leaves and 75 g of soil were added. The sodium bicarbonate was added to mimic the ionic strength of natural systems (Gabor et al. 2015; Wickland et al. 2007) and formaldehyde was added to combat microbial influence (Hader et al. 2003; Soong et al. 2015; Tuominen et al. 1994).

While most of the DOM is leached from soil and leaf litter within the first day (Gunnarsson et al. 1988; Qualls et al. 1991; Steele and Aitkenhead-Peterson 2013), depending on the type of vegetation and conditions this leaching period can be extended to 72 h (McDowell and Fisher 1976) or up to 5 days (Otsuki and Wetzel 1974). A 3-day leach period (July 26–29th, 2019) was chosen to promote leaching of more recalcitrant PyOM compounds. The carboys were loosely covered in foil and stirred frequently. pH, temperature, and conductivity were measured using Hanna probes HI 9025 and HI 9033, respectively. To maintain the pH below 8, hydrochloric acid (HCl) was periodically added to the 400, 550, and 700 °C carboys, totaling 50 mL, 230 mL, and 625 mL, respectively. While organic acids are released during the leaching of natural organic matter, high pH values (> 8.5) have been reported for higher temperature ash leachates because of the denaturing of organic acids accompanied by the release of bases and deposit of alkaline residues (Certini 2005; Wang et al. 2015).

### Photodegradation of leachates

After leaching, all samples were strained through an aluminum mesh and filtered through pre-combusted 0.7  $\mu m$

Whatman GFF filters using Geotech Acrylic Filter towers and peristaltic pumps (Cleveland et al. 2004). Then, 200 mL of filtrate was distributed into 250 mL Nalgene Wide-Mouth PMP (polymethylpentene) Bottles. The PMP bottle material has above 93% transmittance for visible light and outperforms glass and other transparent resins in the UV range with approximate transmittance of 90% for PAR, 75–90% for UVA, 60–75% for UVB (Mitsui Chemicals n.d.). Each burn treatment had six replicate samples for each exposure length of 1, 4, 7, 14, and 25 days, where three replicates were for the dark-controls and three replicates were for light-exposed samples. Day 0 was the only exception with only three replicates for the dark-controlled samples (Supplementary Table 3).

Leachates were placed outside within the protected area of the University of Colorado Boulder's Skywatch Observatory (40°00'40"N, 105°14'32"W) at an elevation of 1660 m and exposed to natural sunlight for exposure times ranging from zero to 25 days starting July 30th until August 23rd, 2019 (Supplementary Fig. 2). The bottles containing the light-exposed leachates were laid sideways on wire racks and the dark-controlled samples were wrapped in aluminum foil and placed in storage bins. All bottles were shaken, flipped, and opened daily. The pH, temperature, and conductivity were checked every day for the first 3 days and then every 3 days for the remainder of the experiment. At the end of each exposure period, samples were filtered through a 0.7  $\mu\text{m}$  pre-combusted GFF filter between the hours of 3–6 PM to ensure light exposure and peroxide generation. The light-exposed samples were filtered on-site and 24 mL of filtrate was immediately added to a dark centrifuge tube containing 1 mL of a reagent to be analyzed for hydrogen peroxide concentrations. The remaining filtrate was transferred to pre-combusted amber glass bottles and stored at 4 °C.

Daily UVB and photosynthetically active radiation (PAR) data were obtained from a nearby NOAA Earth System Research Laboratory (ESRL) Table Mountain site in Boulder, CO. The UVB instrument is a Yankee Environmental Systems model UVB-1 radiometer and the PAR sensor is a LI-COR LI-190R Quantum sensor (Augustine et al. 2000). Daily UVA data were obtained from a Colorado State University Natural Resource Ecology Laboratory (NREL) site in Nunn, CO (elevation 1577 m) (data access at <https://uvb.nrel.colostate.edu/UVB/>) (Gao et al. 2010). The UVA data were collected using an Ultraviolet Multifilter Rotating Shadowband Radiometer (UV-MFRSR). The UVB and PAR data were collected over 24 h. The UVA data were only collected from between 6:00 AM and 6:00 PM. The UVA, UVB, and PAR data were combined and reported as total daily solar radiation. Daily and cumulative solar radiation values can be found in Supplementary Fig. 3 and Supplementary Table 4.

## Laboratory analyses

An Agilent UV–visible spectrophotometer was used to collect absorbance data and a Horiba Jobin Yvon FluoroMax-3 spectrofluorometer equipped with DataMax data acquisition software was used for all fluorescence analysis. Fluorescence analysis was only conducted on one replicate for each temperature and exposure pairing; therefore, 82 EEMs were produced. Prior to any fluorescence analysis, all samples were diluted accordingly to an absorbance below 0.2 at the 254 nm wavelength to prevent inner-filter effects associated with the attenuation of light, which influence the fluorescence signal detected by the fluorometer (Gabor et al. 2014; Cory et al. 2010). Reported UV absorbance ( $UV_{254}$ ) values account for dilutions required to reduce  $UV_{254}$  values to below 0.2 absorbance. The addition of formaldehyde as an antimicrobial agent significantly elevated the total organic carbon data (TOC); therefore, SUVA was not calculated. Formaldehyde has much less of an impact on the  $UV_{254}$ ; therefore,  $UV_{254}$  was used as a proxy for remaining DOM concentration of the leachate instead of TOC.

The photochemical formation of hydrogen peroxide ( $H_2O_2$ ) was quantified by a peroxidase enzyme fluorescent technique adapted from Kok et al. (1986) and Lazrus et al. (1985), which relies on the reaction of  $H_2O_2$ , P-hydroxyphenylacetic acid (pHPAA), and peroxidase to form an easily detectable pHPAA fluorescent dimer. This reaction is complete within 1 min (Kok et al. 1986) and the fluorophore (pHPAA dimer) was measured within 24 h. Given the high concentrations of DOM, high concentrations of  $H_2O_2$  were anticipated and a 1:25 volume dilution of reagent to sample was employed to ensure there was enough pHPAA (Kok et al. 1986). The reagent was prepared fresh for each filtration day and the composition can be found in the Supplementary Materials (Supplementary Table 2). All leachate samples were adjusted to a pH of below 10 using NaOH and diluted to an absorbance below 0.2 using a UV–visible spectrophotometer. A constant wavelength analysis application was used to detect the pHPAA dimer at excitation 320 nm and emission 400 nm. A standard curve was generated using serial dilutions of hydrogen peroxide concentrations (0.05, 0.01, 0.005, 0.001, 0.0005, 0.0001 mM  $H_2O_2$ ) mixed with the reagent, and pH adjusted (> 10).

The 3D EEM scans were collected over the paired excitation–emission wavelengths spanning an excitation range of 240–450 nm at increments of 10 nm and an emission range of 300–550 nm at increments of 2 nm. A blank of distilled water was subtracted from all EEM scans. Matlab was used to instrument correct all EEM scans, normalize with the Raman peak, and compute the following indices. The fluorescence index (FI) is the ratio of emission intensities 470 nm to 520 nm, at an excitation of 370 nm ( $EX_{370}$ ) (Gabor et al. 2014) and indicates the relative contribution of



precursor material from terrestrial or microbial sources. At EX<sub>370</sub>, it is important to note, for natural DOM the maximum emission typically occurs at 470 nm. The humification index (HIX) characterizes the environmental maturation of DOM and is calculated as a ratio of emission signals at excitation 254 nm, where the sum of emission signals from 435 to 480 nm is divided by the sum of emission signals from 330 to 345 nm (Gabor et al. 2014). The freshness index indicates the proportion of recently produced DOM and is calculated as the ratio of emission signals at excitation 310 nm, where emission at 380 nm is divided by the maximum emission intensity with the range of emission signals 420–435 nm (McKnight et al. 2001; Gabor et al. 2014; Hansen et al. 2016). The redox index (RI) characterizes the redox state of quinone-like moieties in humic DOM and is calculated based on components derived from the Cory-McKnight (2005) parallel factor analysis model measuring the sum of reduced quinone-like inputs over total quinone-like inputs (Gabor et al. 2014; Miller et al. 2006, 2009). Index calculations can be found in the Supplemental Materials (Supplementary Table 1).

Statistical analyses and figures were generated in RStudio, Excel, and Matlab. Temporal changes throughout the experiment were fitted with an exponential decay and decay rate and fit measures of  $R^2$  and Residual Standard Error (RSE) were reported. A boxplot comparison was used to summarize the distribution of H<sub>2</sub>O<sub>2</sub> production between the light-exposed and dark-controlled leachates across all temperature treatments. For data that did not meet normality assumptions, the Wilcoxon Rank Sum test was used to determine the significance between the sample populations and median values. When comparing the light-exposed versus dark-controlled samples, there was a right skew; therefore, a one-sided Wilcoxon Rank Sum analysis was used. A principal component analysis (PCA) was used to examine the variation within light-exposed and dark-controlled leachates using the variables of time, treatment temperature, UV absorbance, H<sub>2</sub>O<sub>2</sub> concentration, max emission at EX<sub>370</sub>, and all of the fluorescence indices (FI, HIX, Freshness, and RI).

## Results and discussion

### Photodegradation of the chromophoric fraction of PyDOM

Given that hydrogen peroxide (H<sub>2</sub>O<sub>2</sub>) is a photochemical byproduct of DOM photolysis (Cooper et al. 1988; McKay and Rosario-Ortiz 2015; Scott et al. 2003), the detection of H<sub>2</sub>O<sub>2</sub> indicates that our light-exposed leachates underwent photolysis (Fig. 1). Figure 1a highlights that the production of H<sub>2</sub>O<sub>2</sub> continued decreasing throughout the 25-day experiment in the light-exposed leachates as the available PyDOM

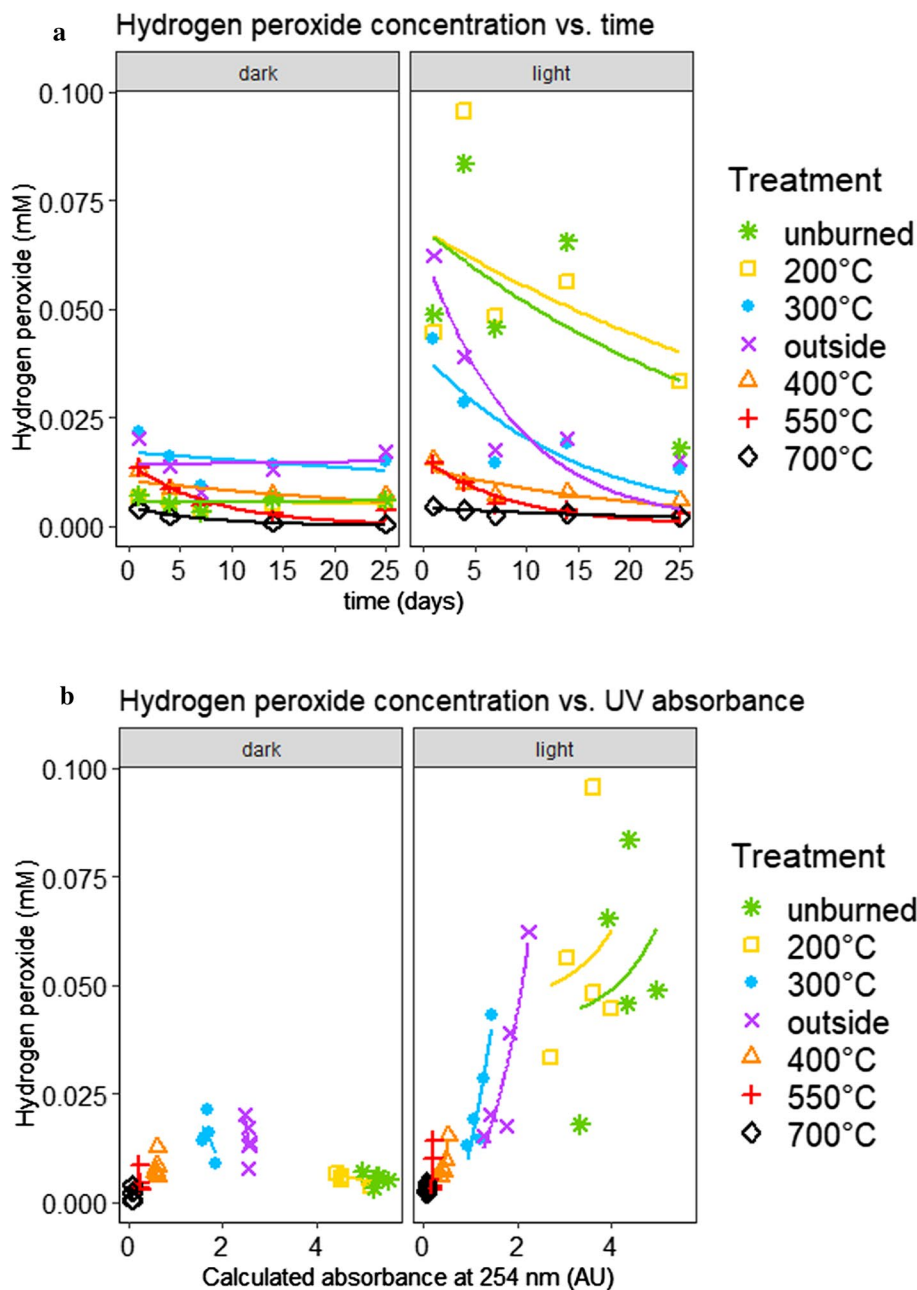
degraded, which is demonstrated in Fig. 1b. Throughout the experiment, UV absorbance (UV<sub>254</sub>) decreased for all light-exposed leachates (Fig. 1b), consistent with previous studies examining PyDOM photoreactivity (Fu et al. 2016; Liu et al. 2022a, b). H<sub>2</sub>O<sub>2</sub> values for the 200, 300 °C, and outside leachates were in a similar range as the unburned control, with lower burn temperature leachates producing more H<sub>2</sub>O<sub>2</sub> and exhibiting higher UV<sub>254</sub>. The higher temperature leachates (400, 550, and 700 °C) exhibited the lowest H<sub>2</sub>O<sub>2</sub> and UV<sub>254</sub> values, potentially indicating the occurrence of less humic acids or macromolecular organic acids than in the lower temperature leachates (Zhang et al. 2020).

For the most part, H<sub>2</sub>O<sub>2</sub> exponentially decayed with time and UV<sub>254</sub> across all light-exposed leachates (Fig. 1). Table 1 lists the exponential decay fit measures for the corresponding plots in Fig. 1. Most of the dark treatments did not generate a decent fit with  $R^2$  values well below 0.5. The exception was the 700 °C leachates which had  $R^2$  values of 0.96 and 0.94 for Fig. 1a and b, respectively. The 700 °C leachates produced the least amount of H<sub>2</sub>O<sub>2</sub> in both exposure groups and also had the lowest UV<sub>254</sub> values, indicating that there was not a large amount of reactive DOM in the highest temperature leachates. The poor fit for the other dark leachates is to be expected given these data are meant to detect photochemical changes by way of H<sub>2</sub>O<sub>2</sub> production. Within the light treatments, the higher temperature leachates (300 °C and above) generally exhibited a better fit to the exponential decay.

Overall, the fits were strongest in the UV<sub>254</sub> and H<sub>2</sub>O<sub>2</sub> plots (Fig. 1b) compared to the temporal plot (Fig. 1a), with all treatments exhibiting  $R^2$  values above 0.88 except for the unburned and 200 °C leachates. This strong relationship reflects that the amount of H<sub>2</sub>O<sub>2</sub> production is dependent on the amount of DOM, where UV<sub>254</sub> is used as a proxy for DOM concentrations. Both the light-exposed unburned and 200 °C treatments exhibited an extremely poor fit ( $R^2 < 0.32$ ) to the exponential decay which is largely because both experienced maximum H<sub>2</sub>O<sub>2</sub> on day 4 and then elevated H<sub>2</sub>O<sub>2</sub> again on day 14. The  $R^2$  metric provides a relative fit measure as a percentage of variance exhibited by the dependent variable (i.e., H<sub>2</sub>O<sub>2</sub>) whereas the residual standard error (RSE) captures the average error in the units of mM H<sub>2</sub>O<sub>2</sub>. Despite the dark leachates having a poor exponential decay fit, nearly all of the RSE values were less than their light-exposed counterparts, emphasizing that overall, there was not much fluctuation in H<sub>2</sub>O<sub>2</sub> within the dark-controlled leachates.

Figure 2 shows side by side boxplot comparisons to highlight the difference between the H<sub>2</sub>O<sub>2</sub> production between light and dark exposure groups across all of the treatments. Nearly all light-exposed groups exhibited a wider range of values with a right skew, reflecting that most light-exposed leachates experienced higher H<sub>2</sub>O<sub>2</sub> production initially and

**Fig. 1** For all burn treatments and light exposures, **a** shows hydrogen peroxide ( $H_2O_2$ ) production throughout the 25-day sun exposure period and **b** shows  $H_2O_2$  production compared to adjusted  $UV_{254}$  absorbance values (accounting for dilution). For each time point, the  $H_2O_2$  and  $UV_{254}$  measurements were made from the same bottle representing the six measurements displayed within each treatment



then as the experiment progressed throughout the 25 days the light-exposed samples degraded, reducing the amount of available DOM, and therefore converged on similar values as the dark leachates. All the light-exposed leachates generally exhibited higher  $H_2O_2$  concentrations compared to their dark counterparts for any given day. The exceptions to this pattern occurred only on the final day 25 for the 300, 400, 550 °C, and outside treatments (Fig. 1a), which likely is a result of the overall reactant DOM pool having been depleted. In all groups, the median  $H_2O_2$  produced by the light group was greater than that of the dark group.

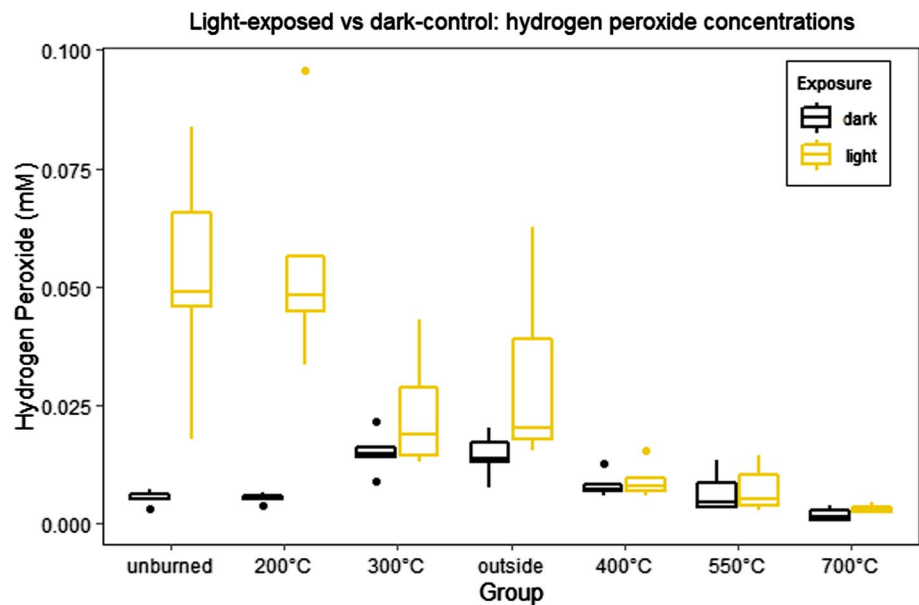
Most of the photodegradation occurred within the first two weeks of the experiment, causing measurements to be skewed. To account for this skew, a one-sided Wilcoxon Rank Sum test was used to determine the significance between the sample populations and median values of the light-exposed versus dark-controlled leachates within each burn treatment. The treatments that differed significantly at a 95% confidence level ( $\alpha = 0.05$ ) were the unburned ( $p = 0.004$ ), 200 °C ( $p = 0.004$ ), and outside ( $p = 0.05$ ) leachates. For the outside treatment, on day 25, the dark leachate exhibited a higher value of  $H_2O_2$  than the light-exposed leachate, whereas on every other

**Table 1** Exponential fit measures for Fig. 1:  $R^2$  values and residual standard error

	a. Time vs. H <sub>2</sub> O <sub>2</sub>				b. Absorbance (UV <sub>254</sub> ) vs. H <sub>2</sub> O <sub>2</sub>			
	Dark		Light		Dark		Light	
	$R^2$	RSE	$R^2$	RSE	$R^2$	RSE	$R^2$	RSE
Unburned	0.01	0.0017	0.32	0.0230	0.13	0.0021	0.13	0.0310
200 °C	0.02	0.0012	0.22	0.0240	0.53	0.0027	0.09	0.0300
300 °C	0.11	0.0048	0.65	0.0079	0.20	0.0055	0.88	0.0084
Outside	0.003	0.0055	0.69	0.0110	0.43	0.0051	0.88	0.0096
400 °C	0.36	0.0025	0.64	0.0025	0.16	0.0027	0.92	0.0032
550 °C	0.75	0.0019	0.86	0.0016	0.64	0.0026	0.93	0.0048
700 °C	0.96	0.0003	0.66	0.0006	0.94	0.0016	0.93	0.0009

\*RSE is in units of mM of H<sub>2</sub>O<sub>2</sub>

**Fig. 2** Distribution of H<sub>2</sub>O<sub>2</sub> concentrations in the light-exposed and dark-controlled leachates across all temperature treatments. Solid lines within the boxplot represent the median (50th percentile), outer edges of the box represent the 25th and 75th percentile, whiskers represent 1.5 times the interquartile range (IQR) under the 25th percentile and over the 75th percentile, and dots represent outliers that exceed the 1.5\*IQR in either direction



day the light-exposed leachates produced much more H<sub>2</sub>O<sub>2</sub> (Fig. 2). The H<sub>2</sub>O<sub>2</sub> distributions and median values across the exposure groups that did not differ significantly included the 300 ( $p=0.2$ ), 400 ( $p=0.4$ ), 550 ( $p=0.4$ ) and 700 °C ( $p=0.1$ ) leachates. Within both exposure groups, the 400 and 550 °C leachates produced similar amounts of H<sub>2</sub>O<sub>2</sub> with the light-exposed leachates producing slightly more on each day except day 25. The light-exposed 700 °C leachates still produced more H<sub>2</sub>O<sub>2</sub> throughout the entire experiment compared to the dark-controls; both groups overall produced smaller amounts of H<sub>2</sub>O<sub>2</sub> and both exhibited an exponential loss of H<sub>2</sub>O<sub>2</sub> throughout the experiment.

Overall, UV<sub>254</sub> values were inversely correlated with treatment temperature, reflecting the associated degree of thermal alteration ( $R^2=0.82$ ,  $p<0.005$ ) (Fig. 3). The average temperature of the outside burn was 388 °C, yet the outside leachates exhibited higher initial UV<sub>254</sub> compared to

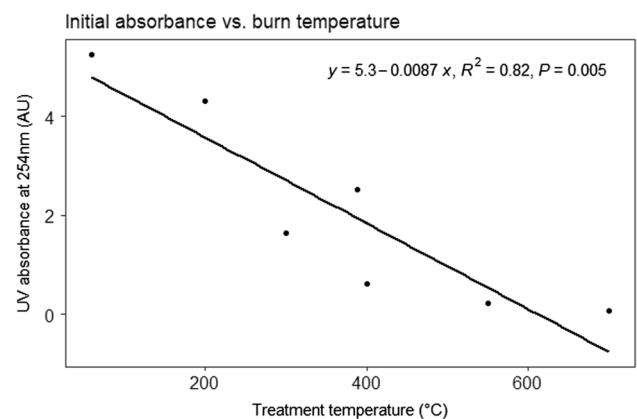


**Fig. 3** Initial comparison (Day 0) of UV<sub>254</sub> absorbance values compared to burn treatment temperatures. The unburned treatment appears at the drying temperature of 60 °C and the outside burn is indicated by the average temperature of 388 °C

both the 300 and 400 °C leachates perhaps indicating uneven burning. Nonetheless, the higher temperature light-exposed leachates experienced a greater decrease in  $UV_{254}$  compared to the dark-controls—indicating photodegradation did occur.

Two significant pairings emerge with the unburned leachates behaving similarly to the leachates of the 200 °C burned material and the leachates of the outside burned material behaving similar to the 300 °C burned material leachates (Fig. 4). The outside and 300 °C pairing indicates that the burn methods employed are relevant to naturally burned OM. In Fig. 4, the data were fit to an exponential decay taking the general form of  $C(t) = C_0e^{-rt}$ , where  $C(t)$  is the amount remaining at time  $t$ ,  $C_0$  is the initial amount, and  $r$  is the exponential decay rate. For the light-exposed leachates, the  $H_2O_2$  decayed at rates of 4 and 5% per day for the 300 °C ( $R^2=0.65$ ) and outside ( $R^2=0.69$ ) treatments, respectively. However, most of the decay happened within the first week and then both treatments exhibited a slight elevation in  $H_2O_2$  on day 14 before declining again on day 25. When looking at the  $UV_{254}$ , the light-exposed groups degraded more slowly at rates of 2 and 2.6% per day for the 300 °C ( $R^2=0.86$ ) and outside ( $R^2=0.87$ ) treatments, respectively. The dark-controlled leachates did not exhibit significant decay in either  $H_2O_2$  ( $R^2=0.11$  for 300 °C and 0.003 for outside) nor  $UV_{254}$  ( $R^2=0.16$  for 300 °C and 0.3 outside), and in fact the outside treatment had a small growth rate rather than decay in both instances.

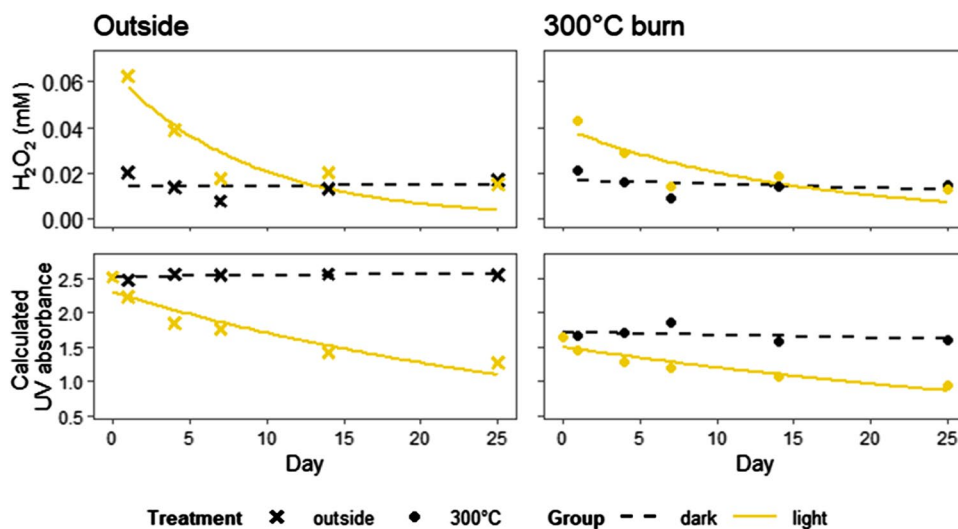
The exponential decay relationships between exposure time and both  $H_2O_2$  concentrations and UV absorbance observed in this experiment emphasizes that short residence times (a few days) decreases the PyDOM. Bostick et al. (2020) reported that 16–22% of PyDOC is readily photomineralized with a less than 1-day half-life while the remaining 78–84% fraction had a half-life around 2 years. Despite these findings, there remains a significant amount of

condensed PyDOM structures detected in rivers and oceans, indicating potential protection mechanisms at play.

### Quantifying photodegradation with fluorescent signatures

Throughout the experiment, the emission intensity of the humic peak for all light-exposed leachates decreased (Fig. 5), with larger decreases in intensity exhibited by the higher temperature leachates ranging from 3.5-fold to 7-fold for the over 300 °C leachates. This decrease in fluorescence intensity is consistent with other studies that used EEMs to evaluate PyDOM photolysis, emphasizing that the higher temperature treatments contained proportionally more chromophoric aromatic and condensed aromatic structures (Bostick et al. 2020; Ward et al. 2014). The dark leachates exhibited no significant change in their fluorescence spectra (see supplemental data). All light-exposed leachates exhibited a decrease in total fluorescence intensity with time. Additionally, higher temperature leachates exhibited lower overall fluorescence intensity, consistent with the findings of Jamieson et al. (2014). The most notable reduction occurred in the humic peak regions (i.e., center of the EEMs). With DOM photodegradation, the reduction in longwave emission is expected and representative of polyaromatic compounds breaking apart and decreasing  $\pi$ -electron system (Coble et al. 2014; Senesi and D’Orazio 2005). The paired decrease in humic peak and increase in shorter wavelengths (referred to as blue-shifting) has also been associated with the formation of new chromophores (Biers et al. 2007; Coble et al. 2014; Fu et al. 2016). Additionally, as polyaromatic compounds continue to degrade, this leads to the reduction of reactive oxygen species (ROS) generated, which aligns with the observed reduction of the  $H_2O_2$  and representative of blue-shifting (Coble et al. 2014; Fu et al. 2016; O’Sullivan

**Fig. 4** Temporal comparison of hydrogen peroxide concentration (mM) and calculated UV absorbance at 254 nm for the outside and 300 °C treatments, including both light-exposed and dark-controlled leachates





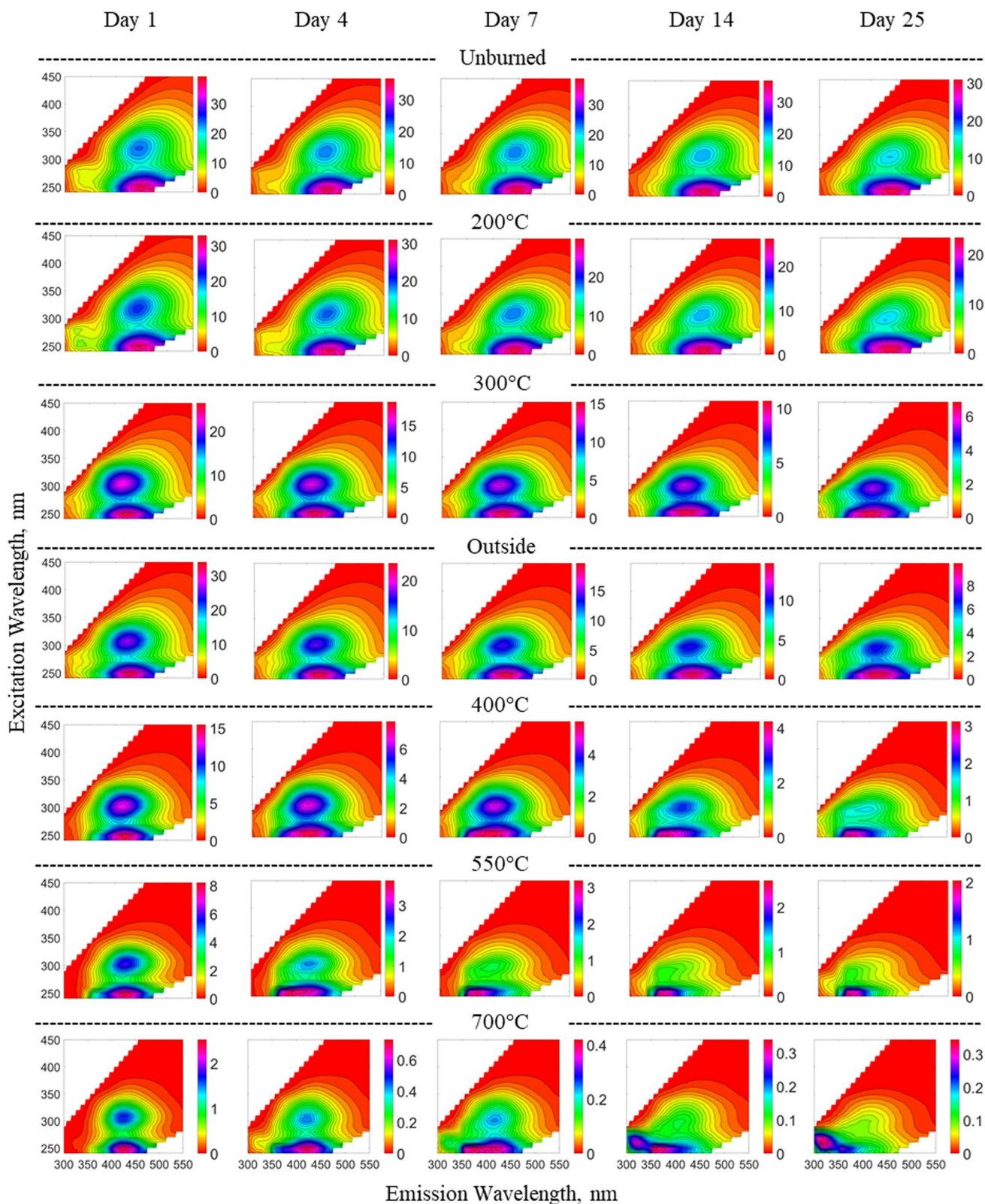


**Fig. 5** Temporal shifts in the EEMs of light-exposed leachates across all burn treatments. Exposure time is increasing left to right and the degree of thermal alteration is increasing top to bottom. Fluorescence intensity is measured in Raman units. All EEMs have the same x- and

y-axes of emission wavelength (300–550 nm) and excitation wavelength (240–450 nm), respectively; however, the intensity scale differs across many of the EEMs. Each EEM was produced from a single sample replicate for that specific treatment and exposure pairing

et al. 2005). Overall, the decrease in  $UV_{254}$ ,  $H_2O_2$  concentrations and the decreased intensity of humic peak indicate photodegradation of PyDOM. These results are consistent with findings from previous studies examining DOM photodegradation (Bostick et al. 2020; Coble et al. 2014; Coble 1996; Moran et al. 2000; Wagner et al. 2018).

An important aspect of our results is that they extend the findings of Bostick et al. (2020) using fluorescence indices to quantify the shifts in EEMs to identify potential measurements for quickly identifying the appearance of PyDOM and potential photochemical changes. The unburned control leachate exhibited a typical FI with maximum emission values at  $EX_{370}$  for natural DOM occurring between 460 and 480 nm (Cory et al. 2007). In contrast, the PyDOM of all the burned leachates, except for 200 °C, exhibited a distinctive fluorescence signature on day zero with emission peaks occurring at or below 450 nm at  $EX_{370}$  (Fig. 6a). With prolonged exposure to sunlight, the emission peaks shifted steadily towards longer wavelengths (red-shifted). This red-shifting has been observed with partial oxidation of

DOM and indicates increasing carboxyl and hydroxyl groups consistent with results from other studies (Coble et al. 2014; Fu et al. 2016; Senesi and D’Orazio 2005; Qu et al. 2016). Nonetheless, the higher temperature leachates of 400, 550, and 700 °C retained an emission peak below 460 nm even by the end of the experiment. The shifted maximum emission values at  $EX_{370}$  (Fig. 6a) influenced the calculated FI values (Fig. 6b). Overall, most FI values were within a normal range for natural DOM, except for the 700 °C leachates that experienced unusually high values ( $> 2$ ) which can be attributed to the lower maximum emission wavelengths at  $EX_{370}$ . While using fluorescence to examine differences in burn severity PyDOM leachates, Wang et al. (2015) also reported that higher temperature leachates exhibited higher FI values; potentially indicating that their samples may have experienced shifted max emission values at  $EX_{370}$ . Throughout the experiment, the dark leachates exhibited an increase in FI while the light-exposed leachates decreased. The higher temperature leachates experienced greater overall decreases in FI: -0.2% (unburned), -3.3% (200 °C), -7.3% (300 °C), -8.4%

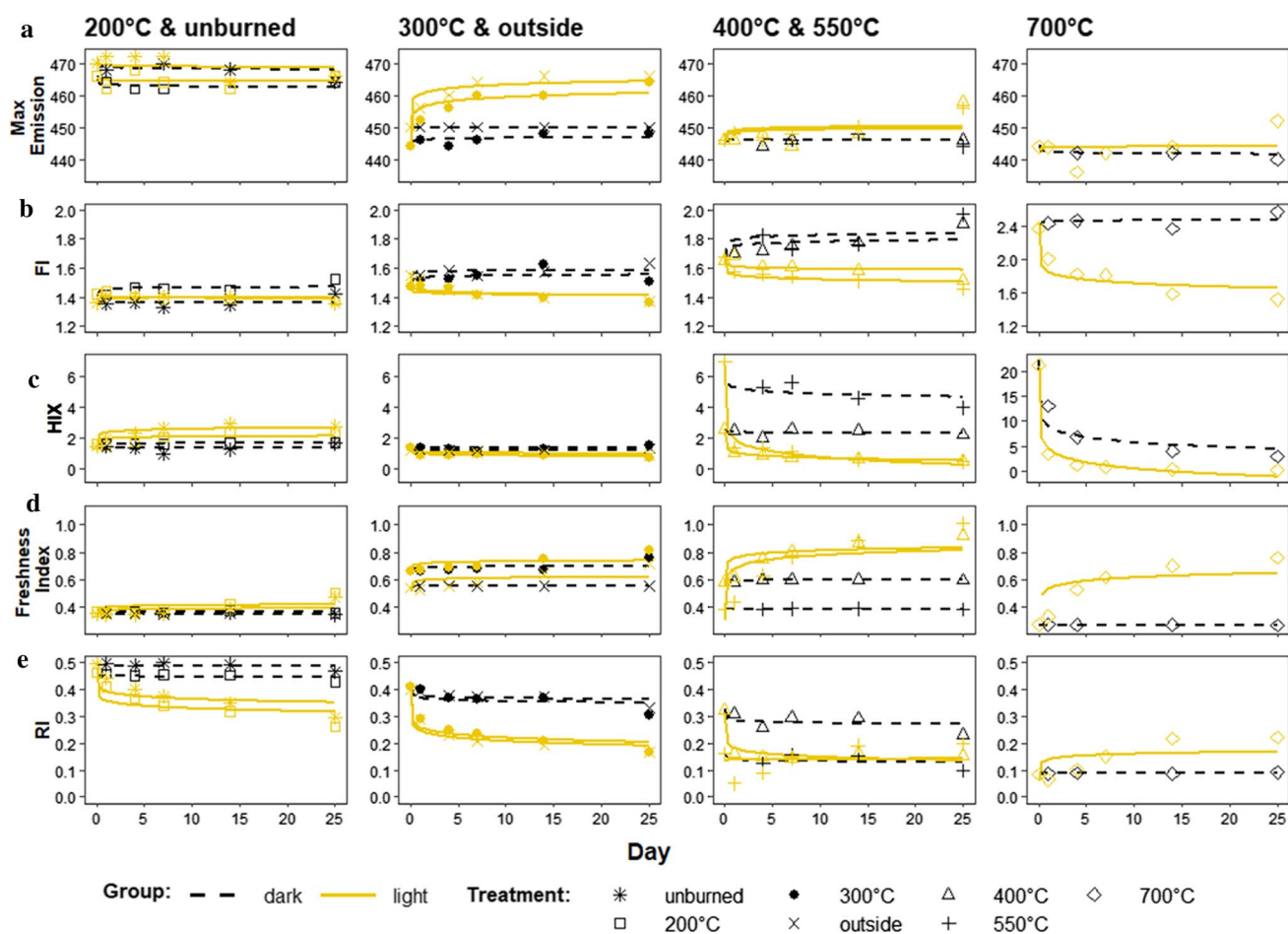


**Fig. 6** Temporal summary of fluorescent signatures across all leachates. The first row **a** shows maximum emission at 370 nm and the remaining rows represent various fluorescence indices over time: **b**—

fluorescence index (FI), **c**—humification index (HIX), **d**—freshness index, and **e**—redox index (RI). All axes' scales are the same except for the HIX and FI maximums for the 700 °C treatment

(400 °C), -11.5% (outside), -13.0% (550 °C), and -35.8% (700 °C). This decrease in FI values with prolonged sunlight exposure has been observed in other DOM photobleaching studies (Hansen et al. 2016; Jaffé et al. 2004). Therefore, the decreasing FI values for the light-exposed leachates are reflective of DOM photobleaching and represent a shifting emission spectrum.

The HIX and Freshness indices typically yield opposite trends. Most of the HIX values were low ( $< 6$ ) (Fig. 6c) compared to the typical 0–30 range for natural OM (NOM). The 700 °C leachates are the exception with values starting at 21.42 and decreasing to 0.14. Higher HIX can be associated with enhanced ring structure (lower H:C ratios), which would explain why the higher temperature leachates exhibited higher HIX values. The rapid decrease in HIX values for the higher temperature leachates could signify a decrease in aromaticity and increase in oxygenated functional groups, which is consistent with the decrease in CDOM and FDOM fractions occurring as a result of photolysis (Ward and Cory 2016). Throughout the experiment, all Freshness index values appeared within a normal range for natural DOM with the light-exposed leachates increasing while the dark leachates remained stable (Fig. 6d). Hansen et al. (2016) also reported an increase in Freshness with increased photoexposure of DOM leachates. Overall, the decrease in HIX and increase in Freshness was likely a result of the diminished humic peak, decrease in fluorescence intensity, and blue-shifting which were evident in the EEMs.

These results are consistent with initially higher FI ( $1.71 \pm 0.03$ ) and HIX ( $24.4 \pm 7.5$ ) values and initially lower Freshness ( $0.89 \pm 0.01$ ) values exhibited by samples analyzed from a recently burned watershed as a result of the Wragg Fire in California (Uzun et al. 2020). Overall, initially high FI, overall lower HIX, and increasing Freshness values could reflect that the leachates were generated from freshly fallen leaves, meaning the parent OM had not yet undergone significant biogeochemical processing (i.e. lacking maturation) compared to older and typical terrestrial DOM signatures (Hansen et al. 2016; Wymore et al. 2015).

Most of the redox index (RI) values were within the lower range for natural DOM ( $< 0.4$ ) (Fig. 6e), indicating that the quinone-like components are more oxidized. The dark leachates remained relatively unchanged, while the light-exposed leachates exhibited variable trends. The lower temperature treatments (unburned, 200, 300, and 400 °C) exhibited a further decrease in RI values throughout the experiment, indicating the PyDOM is becoming increasingly degraded and oxidized. Whereas the 500 and 700 °C samples exhibited an increase in RI values with increased sun exposure, perhaps indicative that new and reduced compounds were being generated. This would align with the skewed humic peak observed in the EEMs

of these temperature treatments (Fig. 5). Photooxidation can cause aromatic rings to open, which disrupts charge transfer reactions, resulting in longer wavelength absorption and fluorescence (Osburn et al. 2014; Del Vecchio and Blough 2004). Our results could be reflective of intermediate products, including ROS, typically known to occur with DOM photolysis, which can assist in subsequent reactions that can further oxidize or reduce DOM (Fu et al. 2016; Osburn et al. 2014). This similar reducing result was observed in Klapper et al. (2002) who reported that within a degrading environment microbial electron transfers can result in a shift of the main humic fluorophores to higher emission wavelengths. Yan et al. (2022) reported that their higher temperature PyDOM (450 °C) experienced more photodegradation on a longer timescale (30 days), suggesting that the increased production of ROS facilitated the transformation of condensed aromatics into aliphatics, proteins, and tannins. While  $\text{H}_2\text{O}_2$  production was detected, future work would be needed to determine apparent quantum yields and ROS production to better quantify photochemical changes (Fu et al. 2016; Y. Liu et al. 2022a, b; Wang et al. 2020).

The variables of time (day), treatment temperature,  $\text{UV}_{254}$ ,  $\text{H}_2\text{O}_2$  concentration, max emission at  $\text{EX}_{370}$  (Max EM), and all of the fluorescence indices (FI, HIX, Freshness, and RI) were used in a principal component analysis (PCA) to examine the variation within the light-exposed and dark-controlled leachate groups (Fig. 7). Within the light-exposed group, there was a clear association between treatment temperature and PC1, while PC2 showed a strong association with time. PC1 and PC2 together accounted for 82.7% of the total variance. PC1 accounted for 61% of the explained variance and the variables most strongly correlated (positive) or anti-correlated (negative) with PC1 being  $\text{UV}_{254}$  (-0.420 loading), treatment temperature (0.389), RI (-0.383),  $\text{H}_2\text{O}_2$  (-0.374), and Max EM (-0.368). PC2 accounted for 21.7% of the explained variance and the variables most strongly correlated/anticorrelated with PC2 include time (-0.584), FI (0.483), freshness index (-0.451), and HIX (0.321). Within the dark-controlled group, there remained a clear association with treatment temperature for PC1; however, as we would expect, changes within the fluorescence signatures and  $\text{H}_2\text{O}_2$  were no longer correlated with time. PC1 and PC2 together accounted for 79.9% of the total variance. PC1 accounted for 55.4% of the explained variance with the variables most strongly correlated/anticorrelated with PC1 being RI (-0.437), treatment temperature (0.437), FI (0.418), UV (-0.405), Max EM (-0.377), and HIX (0.337). PC2 accounted for 24.5% of explained variance with the most strongly correlated/anticorrelated variables being freshness index (-0.636),  $\text{H}_2\text{O}_2$  (-0.578), and Max EM (0.348). Overall,



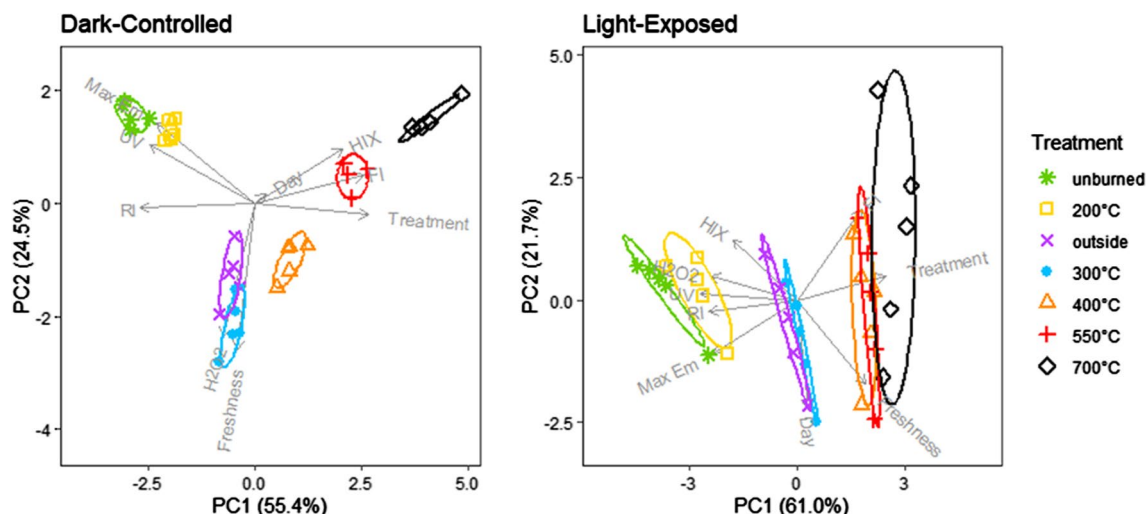


**Fig. 7** Principal component analysis examining the variation within dark-controlled and light-exposed leachates, using the variables of time (Day), treatment temperature (Treatment), UV absorbance (UV), H<sub>2</sub>O<sub>2</sub> concentration (H<sub>2</sub>O<sub>2</sub>), max emission at EX<sub>370</sub> (Max Em), and

all of the fluorescence indices (FI, HIX, Freshness, and RI). The unburned treatment appears at the drying temperature of 60 °C and the outside burn is indicated by the average temperature of 388 °C

**Table 2** Summary of fluorescence results and comparison to photodegraded NOM

Index	Experimental results for photodegraded PyDOM	Typical results for photodegraded NOM
Max EM	Higher thermal alteration led to <b>lower</b> values (< 450 nm) Photolysis caused values to increase	Values usually remain around 470 nm <sup>a</sup>
FI	Higher thermal alteration led to <b>higher</b> values Photolysis caused values to decrease	Values usually remain < 2 <sup>a</sup> Photolysis typically causes either no change or decreasing values <sup>a,b,c,d</sup>
HIX	Values overall lower, except higher thermal alteration led to <b>higher</b> values Photolysis caused values to decrease	Values usually between 0-30. Lower values typical for less mature NOM <sup>b</sup> Typical photolysis trend <sup>c</sup>
Freshness	Values within <b>normal</b> range Photolysis caused values to increase, especially for higher temperature leachates	Values typical of freshly produced NOM Typical photolysis trend <sup>c</sup>
RI	Higher thermal alteration led to <b>lower</b> values Photolysis caused mixed results. Values for higher temperature leachates increased, while the rest decreased	Values usually around 0.4. Lower values consistent for NOM that is more oxidized <sup>b</sup> Photolysis typically causes decreasing values

<sup>a</sup>Cory et al. (2007)

<sup>b</sup>Gabor et al. (2014)

<sup>c</sup>Hansen et al. (2016)

<sup>d</sup>Jaffé et al. (2004)

both dark-controlled and photodegraded PyDOM exhibited distinct relationships across fluorescence signatures.

**Fluorescence index summary and comparison to natural organic matter (NOM)**

Table 2 provides a comparison of the results from the PyDOM photoexposure experiment to typical photodegraded NOM. Overall, these results show how PyDOM can be photodegraded to exhibit fluorescence signatures resembling NOM.

Some differences unique to the higher temperature leachates include initially lower Max EM, higher FI, and lower RI values. Whereas initial HIX and Freshness values for the higher temperature leachates were within expected ranges for less mature NOM—likely a result of using freshly fallen leaf litter as the parent OM. In terms of expected trends, the decrease in HIX and increase in Freshness is typically observed with photodegraded NOM (Hansen et al. 2016). The observed shifts of the Max EM values towards longer wavelengths and FI to lower values could indicate that the



photodegradation of PyDOM increases the likelihood that burned leachates can return to more typical values resembling natural DOM with increased sun exposure, likely representing the transformation of condensed aromatics into aliphatics, proteins, and tannins (Yan et al. 2022). This return to natural DOM signatures has also been documented in a hydrologic flushing study, where unique DOM wildfire fluorescence signatures exhibited pronounced short-term (< 1 year) signatures but with repeated flushing and time the DOM fluorescent characteristics resembled reference watershed values (Uzun et al. 2020).

Therefore, higher temperature leachates tend to exhibit distinctive differences from what would typically be observed for NOM. However, as these higher temperature PyDOM leachates experience prolonged exposure to solar radiation, the fluorescence signatures trend towards signatures that resemble NOM. These distinct signals and trends could assist in identifying instream wildfire signals in both the short and long-term depending on the pathways and sun exposure PyOM encounters.

## Conclusion

The production of hydrogen peroxide, the decrease in UV absorbance, and the observed shifts in fluorescence signatures indicated that the PyDOM was photochemically altered throughout the 25-day solar radiation exposure period extending the findings of previous studies of PyDOM photodegradation potential (Bostick et al. 2020; Fu et al. 2016; Liu et al. 2022a, b; Stubbins et al. 2012; Ward et al. 2014; Wagner et al. 2018; Wagner and Jaffe 2015; Yan et al. 2022). While some studies used fluorescence more broadly to identify unique PyDOM signatures, our study demonstrates the value of using fluorescence indices to capture PyDOM composition over a wide range of pyrolysis temperatures. Higher burn temperatures resulted in distinctive fluorescence characteristics with PyDOM that exhibited lower overall fluorescence intensity, a distinctive lower max emission peak (< 460 nm) at EX<sub>370</sub>, higher FI values (around or above 2), higher HIX values (> 10), and lower RI values (< 0.4). With increased exposure to sunlight, the higher temperature leachates begin to exhibit fluorescence values that resemble unburned NOM. These results reveal that burn severity is an important factor influencing the fluorescence characteristics and trends of PyDOM and could contribute to the extent of PyDOM photo-transformations as shown in Goranov et al. (2020) and Bostick et al. (2020). Throughout all the analyses, the outside burn and 300 °C muffle furnace burn exhibited similar results, indicating that the results of the various temperature leachates within this study are relevant to naturally burned OM. The temporal decrease in H<sub>2</sub>O<sub>2</sub>

concentrations exhibited by the light-exposed burn leachates provides direct chemical evidence that the labile fraction of PyDOM can be significantly reduced by photodegradation. In the presence of sunlight, PAHs are susceptible to being oxidized with some resulting photoproducts being more biodegradable, so further research would be needed to assess the additional influence of microbes. Bostick et al. (2021) has recently shown that photodegraded PyDOM is more susceptible to being biomineralized, but this availability varies and should be examined in natural systems.

Our results show that with prolonged exposure to solar radiation, PyDOM compounds are not only susceptible to photodegradation but also exhibit fluorescence signatures that resemble NOM over time. This finding indicates that perhaps downstream water treatment plants (WTP) might benefit from PyDOM remaining in natural surface waters for extended periods of time prior to entering the facility. Conversely if the DOM exhibit distinct fluorescence signatures following wildfire inputs, this might indicate the presence of more condensed PyDOM and warrant additional or different treatment strategies to avoid the formation of DBPs. Wang et al. (2015) reported that higher temperature leachates resulted in a reduction of carbonaceous DBP precursors but a significant increase in the more toxic nitrogenous specific DBPs formation potential. The interactions between PyDOM, photolysis, and DBP formation should be explored further.

This study demonstrates that photodegradation alters the fluorescence signature of PyDOM, contributing to growing evidence that PyOM is reactive in the environment (Bostick et al. 2020; Fu et al. 2016; Liu et al. 2022a, b; Stubbins et al. 2012; Wagner et al. 2018; Wagner and Jaffe 2015; Ward et al. 2014; Yan et al. 2022). The projected increase in intensity and frequency of wildfires (Abatzoglou and Williams 2016) are likely to increase the amount of pyrogenic carbon produced creating implications for carbon cycling, carbon sequestration, ecological consequences, and health risks (Bostick et al. 2020; Yan et al. 2022); therefore, identifying, and characterizing PyOM fate and transport is needed for water quality management. Because fluorescence spectroscopy is becoming increasingly utilized by WTP operators due to its quick analysis time and small sample volume requirement, certain fluorescence signatures (like the characteristically low emission peak) could prove useful to WTP operators for detecting fresh PyDOM. Furthermore, these photo-exposure results highlight how fluorescence can be a meaningful tool in detecting or explaining wildfire signatures compared to NOM. Overall, these results demonstrate that bulk PyDOM derived from burned leachates is susceptible to photodegradation and that fluorescence measurements could be used as proxies for detecting PyDOM immediately post-wildfire or explaining temporal and downstream shifts.

**Supplementary Information** The online version contains supplementary material available at <https://doi.org/10.1007/s00027-022-00919-7>.

**Acknowledgements** The authors would like to thank the Great Smoky Mountain National Park (GRSMNP) staff for their support of the fieldwork which was conducted and authorized under permit GRSM-2018-SCI-2051. We thank A. Turner for laboratory assistance and N. Schulte for guidance with the statistical analyses. Funding for the project was provided by the National Science Foundation RAPID grant #1733885. NEON is sponsored by the National Science Foundation and operated under cooperative agreement by Battelle. This material is based in part upon work supported by NSF through the NEON Program. All sample preparation and analysis occurred within the Organic Matter Spectroscopy and Sedimentology Laboratories at the University of Colorado Boulder located in Boulder, CO. The outdoor portion of the experiment was housed within the University of Colorado Boulder's Skywatch Observatory.

**Data availability** The datasets generated during and/or analyzed during the current study are available from the corresponding author upon reasonable request.

## Declarations

**Conflict of interest** Partial financial support was received from the National Science Foundation RAPID grant #1733885.

**Open Access** This article is licensed under a Creative Commons Attribution 4.0 International License, which permits use, sharing, adaptation, distribution and reproduction in any medium or format, as long as you give appropriate credit to the original author(s) and the source, provide a link to the Creative Commons licence, and indicate if changes were made. The images or other third party material in this article are included in the article's Creative Commons licence, unless indicated otherwise in a credit line to the material. If material is not included in the article's Creative Commons licence and your intended use is not permitted by statutory regulation or exceeds the permitted use, you will need to obtain permission directly from the copyright holder. To view a copy of this licence, visit <http://creativecommons.org/licenses/by/4.0/>.

## References

- Abatzoglou JT, Williams AP (2016) Impact of anthropogenic climate change on wildfire across western US forests. *Proc Natl Acad Sci* 113:11770–11775. <https://doi.org/10.1073/pnas.1607171113>
- Abrajano TA, Yan B, Song J, Bopp R, O'Malley V (2007) High-molecular-weight petrogenic and pyrogenic hydrocarbons in aquatic environments. In: Holland HD, Turekian KK (eds) *Treatise on geochemistry* pergamon, Oxford, pp 1–50. <https://doi.org/10.1016/B0-08-043751-6/09055-1>
- Augustine JA, Deuisi JJ, Long CN (2000) SURFRAD—a national surface radiation budget network for atmospheric research. *Bull Am Meteorol Soc* 81:2341–2358. [https://doi.org/10.1175/1520-0477\(2000\)081%3c2341:SANSRB%3e2.3.CO;2](https://doi.org/10.1175/1520-0477(2000)081%3c2341:SANSRB%3e2.3.CO;2)
- Baker A (2001) Fluorescence excitation–emission matrix characterization of some sewage-impacted rivers. *Environ Sci Technol* 35:948–953. <https://doi.org/10.1021/es000177t>
- Bedell E, Harmon O, Fankhauser K, Shivers Z, Thomas E (2022) A continuous, in-situ, near-time fluorescence sensor coupled with a machine learning model for detection of fecal contamination risk in drinking water: design, characterization and field validation. *Water Res* 220:118644. <https://doi.org/10.1016/j.watres.2022.118644>
- Biers EJ, Zepp RG, Moran MA (2007) The role of nitrogen in chromophoric and fluorescent dissolved organic matter formation. *Marine Chem* 103:46–60. <https://doi.org/10.1016/j.marchem.2006.06.003>
- Bird MI, Wynn JG, Saiz G, Wurster CM, McBeath A (2015) The pyrogenic carbon cycle. *Ann Review of Earth Planetary Sci* 43:273–298. <https://doi.org/10.1146/annurev-earth-060614-105038>
- Blank RR, Allen F, Young JA (1994) Extractable anions in soils following wildfire in a sagebrush-grass community. *Soil Sci Soc of Am J* 58(2):564–570. <https://doi.org/10.2136/sssaj1994.03615995005800020045x>
- Blank RR, Allen F, Young JA (1996) Influence of simulated burning of soil-litter from low sagebrush, squirrel tail, cheatgrass, and medusahead on water-soluble anions and cations. *Int J Wildland Fire* 6:137–143
- Bostick KW, Zimmerman AR, Wozniak AS, Mitra S, Hatcher PG (2018) Production and composition of pyrogenic dissolved organic matter from a logical series of laboratory-generated chars. *Front Earth Sci* 6:43. <https://doi.org/10.3389/feart.2018.00043>
- Bostick KW, Zimmerman AR, Goranov AI, Mitra S, Hatcher PG, Wozniak AS (2020) Photolability of pyrogenic dissolved organic matter from a thermal series of laboratory-prepared chars. *Sci Total Environ* 724:138198. <https://doi.org/10.1016/j.scitotenv.2020.138198>
- Bostick KW, Zimmerman AR, Goranov AI, Mitra S, Hatcher PG, Wozniak AS (2021) Biolability of fresh and photodegraded pyrogenic dissolved organic matter from laboratory-prepared chars. *J Geophys Res* 126(5):5e2020JG005981. <https://doi.org/10.1029/2020JG005981>
- Brown RA, Kercher AK, Nguyen TH, Nagle DC, Ball WP (2006) Production and characterization of synthetic wood chars for use as surrogates for natural sorbents. *Organic Geochem* 37:321–333. <https://doi.org/10.1016/j.orggeochem.2005.10.008>
- Buechi H, Weber P, Heard S, Cameron D, Plantinga AJ (2021) Long-term trends in wildfire damages in California. *Int J Wildland Fire* 30:757–762. <https://doi.org/10.1071/WF21024>
- Certini G (2005) Effects of fire on properties of forest soils: a review. *Oecologia* 143:1–10. <https://doi.org/10.1007/s00442-004-1788-8>
- Cleveland CC, Neff JC, Townsend AR, Hood E (2004) Composition, dynamics, and fate of leached dissolved organic matter in terrestrial ecosystems: results from a decomposition experiment. *Ecosystems* 7:175–285. <https://doi.org/10.1007/s10021-003-0236-7>
- Coble PG (1996) Characterization of marine and terrestrial DOM in seawater using excitation-emission matrix spectroscopy. *Marine Chem* 51:325–346. [https://doi.org/10.1016/0304-4203\(95\)00062-3](https://doi.org/10.1016/0304-4203(95)00062-3)
- Coble P, Lead J, Baker A, Reynolds DM, Spencer RG, eds. (2014) *Aquatic organic matter fluorescence*. Cambridge Environmental Chemistry Series. New York, Cambridge University Press
- Cooper WJ, Zika RG, Petasne RG, Plane JMC (1988) Photochemical formation of hydrogen peroxide in natural waters exposed to sunlight. *Environ Sci Technol* 22:1156–1160. <https://doi.org/10.1021/es00175a004>
- Cory RM, McKnight DM (2005) Fluorescence spectroscopy reveals ubiquitous presence of oxidized and reduced quinones in dissolved organic matter. *Environ Sci Technol* 39:8142–8149. <https://doi.org/10.1021/es0506962>
- Cory RM, McKnight DM, Chin Y, Miller P, Jaros CL (2007) Chemical characteristics of fulvic acids from arctic surface waters: microbial contributions and photochemical transformations. *J Geophys Res Biogeosci*. <https://doi.org/10.1029/2006JG000343>
- Cory RM, Miller MP, McKnight DM, Guerard JJ, Miller P (2010) Effect of instrument-specific response on the analysis of fulvic acid fluorescence spectra. *Limnol Oceanogr* 8:67–78. <https://doi.org/10.4319/lom.2010.8.67>

- Creed IF, McKnight DM, Pellerin BA, Green MB, Bergamaschi BA, Aiken GR, Burns DA et al (2015) The river as a chemostat: fresh perspectives on dissolved organic matter flowing down the river continuum. *Can J Fish Aquat Sci* 72:1272–1285. <https://doi.org/10.1139/cjfas-2014-0400>
- Del Vecchio R, Blough NV (2004) On the origin of the optical properties of humic substances. *Environ Sci Technol* 38(14):3885–3891. <https://doi.org/10.1021/es049912h>
- Dittmar T, de Rezende CE, Manecki M, Niggemann J, Coelho Ovalle AR, Stubbins A, Bernardes MC (2012) Continuous flux of dissolved black carbon from a vanished tropical forest biome. *Nature Geosci* 5:618–622. <https://doi.org/10.1038/ngeo1541>
- Fasnacht MP, Blough NV (2002) Aqueous photodegradation of polycyclic aromatic hydrocarbons. *Environ Sci Technol* 36(20):4364–4369. <https://doi.org/10.1021/es025603k>
- Freeman MC, Pringle CM, Jackson CR (2007) Hydrologic connectivity and the contribution of stream headwaters to ecological integrity at regional scales. *J Am Water Resour Assoc* 43:5–14. <https://doi.org/10.1111/j.1752-1688.2007.00002.x>
- Fu H, Liu H, Mao J, Chu W, Li Q, Alvarez PJJ, Qu X, Zhu D (2016) Photochemistry of dissolved black carbon released from biochar: reactive oxygen species generation and phototransformation. *Environ Sci Technol* 50:1218–1226. <https://doi.org/10.1021/acs.est.5b04314>
- Gabor RS, Baker A, McKnight DM, Miller MP (2014) Fluorescence indices and their interpretation. In: Coble P, Lead J, Baker A, Reynolds DM, Spencer RG (eds) *Aquatic organic matter fluorescence*, Cambridge environmental chemistry series. Cambridge University Press, New York, pp 303–338
- Gabor RS, Burns MA, Lee RH, Elg JB, Kemper CJ, Barnard HR, McKnight DM (2015) Influence of leaching solution and catchment location on the fluorescence of water-soluble organic matter. *Environ Sci Technol* 49:4425–4432. <https://doi.org/10.1021/es04881t>
- Gao W, Davis JM, Tree R, Slusser JR, Schmoltdt D (2010) An ultraviolet radiation monitoring and research program for agriculture. In: Gao E, Slusser JR, Schmoltdt DL (eds) *UV radiation in global climate change: measurements, modeling and effects on ecosystems*. Springer, Berlin, Heidelberg, pp 205–243. [https://doi.org/10.1007/978-3-642-03313-1\\_8](https://doi.org/10.1007/978-3-642-03313-1_8)
- Goranov AI, Wozniak AS, Bostick KW, Zimmerman AR, Mitra S, Hatcher PG (2020) Photochemistry after fire: structural transformations of pyrogenic dissolved organic matter elucidated by advanced analytical techniques. *Geochim Cosmochim Acta* 290:271–292. <https://doi.org/10.1016/j.gca.2020.08.030>
- Gunnarsson T, Sundin P, Tunlid A (1988) Importance of leaf litter fragmentation for bacterial growth. *Oikos* 52(3):303–308. <https://doi.org/10.2307/3565203>
- Hader D, Jori G, Webb AR, Neale PJ, Kieber DJ, Wetzel RG, Blumthaler M, et al. (2003) In: Walter Helbling EW, Zagares H (eds) *UV Effects in aquatic organisms and ecosystems*. Comprehensive series in photochemical & photobiological sciences. The Royal Society of Chemistry. <https://doi.org/10.1039/9781847552266>
- Hansen AM, Kraus TEC, Pellerin BA, Fleck JA, Downing BD, Bergamaschi BA (2016) Optical properties of dissolved organic matter (DOM): effects of biological and photolytic degradation. *Limnol Oceanogr* 61:1015–1032. <https://doi.org/10.1002/lno.10270>
- Harvey BJ (2016) Human-caused climate change is now a key driver of forest fire activity in the western united states. *Proc National Acad Sci* 113:11649–11650. <https://doi.org/10.1073/pnas.1612926113>
- Hockaday WC, Grannas AM, Kim S, Hatcher PG (2007) The transformation and mobility of charcoal in a fire-impacted watershed. *Geochim Cosmochim Acta* 71:3432–3445. <https://doi.org/10.1016/j.gca.2007.02.023>
- Jaffé R, Boyer JN, Lu X, Maie N, Yang C, Scully NM, Mock S (2004) Source characterization of dissolved organic matter in a subtropical mangrove-dominated estuary by fluorescence analysis. *Marine Chem* 84:195–210. <https://doi.org/10.1016/j.marchem.2003.08.001>
- Jamieson T, Sager E, Guéguen C (2014) Characterization of biochar-derived dissolved organic matter using UV–visible absorption and excitation–emission fluorescence spectroscopies. *Chemosphere* 103:197–204. <https://doi.org/10.1016/j.chemosphere.2013.11.066>
- Klapper L, McKnight DM, Fulton JR, Blunt-Harris EL, Nevin KP, Lovley DR, Hatcher PG (2002) Fulvic acid oxidation state detection using fluorescence spectroscopy. *Environ Sci Technol* 36:3170–3175. <https://doi.org/10.1021/es0109702>
- Kok GL, Thompson K, Lazrus AL, McLaren SE (1986) Derivatization technique for the determination of peroxides in precipitation. *Anal Chem* 58:1192–1194. <https://doi.org/10.1021/ac00297a047>
- Lazrus AL, Kok GL, Gitlin SN, Lind JA, McLaren SE (1985) Automated fluorimetric method for hydrogen peroxide in atmospheric precipitation. *Anal Chem* 57:917–922. <https://doi.org/10.1021/ac00281a031>
- Liu N, Dobbs GR, Caldwell PV, Miniati CF, Sun G, Duan K, Nelson SAC, Bolstad PV, Carlson CP (2022a) Quantifying the role of National Forest System and other forested lands in providing surface drinking water supply for the conterminous United States (General Technical Report No. WO-100). U.S. Department of Agriculture, Forest Service. <https://doi.org/10.2737/WO-GTR-100>
- Liu Y, Wang M, Yin S, Xie L, Qu X, Fu H, Shi Q, Zhou F, Xu F, Tao S, Zhu D (2022b) Comparing photoactivities of dissolved organic matter released from rice straw-pyrolyzed biochar and composted rice straw. *Environ Sci Technol* 56:2803–2815. <https://doi.org/10.1021/acs.est.1c08061>
- Matosziuk LM, Gallo A, Hatten J, Bladon KD, Ruud D, Bowman M, Egan J et al (2020) Short-term effects of recent fire on the production and translocation of pyrogenic carbon in Great Smoky Mountains National Park. *Front Forests Glob Change*. <https://doi.org/10.3389/ffgc.2020.00006>
- McDowell WH, Fisher SG (1976) Autumnal processing of dissolved organic matter in a small woodland stream ecosystem. *Ecology* 57:561–569. <https://doi.org/10.2307/1936440>
- McKay G, Rosario-Ortiz FL (2015) Temperature dependence of the photochemical formation of hydroxyl radical from dissolved organic matter. *Environ Sci Technol* 49:4147–4154. <https://doi.org/10.1021/acs.est.5b00102>
- McKnight DM, Boyer EW, Westerhoff PK, Doran PT, Kulbe T, Andersen DT (2001) Spectrofluorometric characterization of dissolved organic matter for indication of precursor organic material and aromaticity. *Limnol Oceanogr* 46:38–48. <https://doi.org/10.4319/lo.2001.46.1.0038>
- Miller MP, McKnight DM, Cory RM, Williams MW, Runkel RL (2006) Hyporheic exchange and fulvic acid redox reactions in an alpine stream/wetland ecosystem, Colorado Front Range. *Environ Sci Technol* 40:5943–5949. <https://doi.org/10.1021/es060635j>
- Miller MP, McKnight DM, Chapra S, Williams MW (2009) A model of degradation and production of three pools of dissolved organic matter in an alpine lake. *Limnol Oceanogr* 54:2213–2227. <https://doi.org/10.4319/lo.2009.54.6.2213>
- Mitsui Chemicals (n.d) TPXTM, Polymethylpentene (PMP). Mitsui Chem. Am. Inc. <https://us.mitsuichemicals.com/service/product/tpx.htm>. Accessed 24 Oct 2022
- Moran MA, Sheldon WM, Zepp RZ (2000) Carbon loss and optical property changes during long-term photochemical and biological degradation of estuarine dissolved organic matter. *Limnol Oceanogr* 45:1254–1264. <https://doi.org/10.4319/lo.2000.45.6.1254>
- Myers-Pigg AN, Louchouart P, Amon RMW, Prokushkin A, Pierce AK, Rubtsov A (2015) Labile pyrogenic dissolved organic carbon



- in major Siberian arctic rivers: implications for wildfire-stream metabolic linkages. *Geophysical Res Lett* 42:377–385. <https://doi.org/10.1002/2014GL062762>
- Myers-Pigg AN, Louchouart P, Teisserenc R (2017) Flux of dissolved and particulate low-temperature pyrogenic carbon from two high-latitude rivers across the spring freshet hydrograph. *Front Mar Sci*. <https://doi.org/10.3389/fmars.2017.00038>
- National Park Service (NPS) (2019) Trees and Shrubs Checklist - Great Smoky Mountains National Park (U.S. National Park Service). <https://www.nps.gov/grsm/learn/nature/trees-shrubs-list.htm>. Accessed 17 Jun 2020
- Novotny EH, de Freitas Maia CMB, de Melo Carvalho MT, Madari BE (2015) Biochar: pyrogenic carbon for agricultural use—a critical review. *Rev Bras Ciênc Solo* 39(2):321–344. <https://doi.org/10.1590/01000683rbc20140818>
- O'Sullivan DW, Neale PJ, Coffin RB, Boyd TJ, Osburn CL (2005) Photochemical production of hydrogen peroxide and methylhydroperoxide in coastal waters. *Marine Chem* 97:14–33. <https://doi.org/10.1016/j.marchem.2005.04.003>
- Osburn CL, Del Vecchio R, Boyd TJ (2014) Physicochemical effects on dissolved organic matter fluorescence in natural waters. In: Coble P, Lead J, Baker A, Reynolds DM, Spencer RG (eds) *Aquatic organic matter fluorescence*, Cambridge environmental chemistry series. Cambridge University Press, New York, pp 233–277
- Otsuki A, Wetzel RG (1974) Release of dissolved organic matter by autolysis of a submersed macrophyte, *Scirpus subterminalis*. *Limnol Oceanogr* 19:842–845. <https://doi.org/10.4319/lo.1974.19.5.0842>
- Pagni RM, Sigman ME (1999) The photochemistry of PAHs and PCBs in water and on solids. In Boule P (ed) *Environmental photochemistry, The Handbook of Environmental Chemistry*. Springer, Berlin, Heidelberg, pp 139–79. [https://doi.org/10.1007/978-3-540-69044-3\\_6](https://doi.org/10.1007/978-3-540-69044-3_6)
- Qu X, Fu H, Mao J, Ran Y, Zhang D, Zhu D (2016) Chemical and structural properties of dissolved black carbon released from biochars. *Carbon* 96:759–767. <https://doi.org/10.1016/j.carbon.2015.09.106>
- Qualls RG, Haines BL, Swank WT (1991) Fluxes of dissolved organic nutrients and humic substances in a deciduous forest. *Ecology* 72:254–266. <https://doi.org/10.2307/1938919>
- Roebuck JA, Seidel M, Dittmar T, Jaffé R (2018) Land use controls on the spatial variability of dissolved black carbon in a subtropical watershed. *Environ Sci Technol* 52(15):8104–8114. <https://doi.org/10.1021/acs.est.8b00190>
- Santín C, Doerr SH, Merino A, Bucheli TD, Bryant R, Ascough PA, Gao X, Masiello CA (2017) Carbon sequestration potential and physicochemical properties differ between wildfire charcoals and slow-pyrolysis biochars. *Sci Rep*. <https://doi.org/10.1038/s41598-017-10455-2>
- Schneider MPW, Hil M, Vogt UF, Schmidt MWI (2010) The benzene polycarboxylic acid (BPCA) pattern of wood pyrolyzed between 200°C and 1000°C. *Organic Geochem* 41:1082–1088. <https://doi.org/10.1016/j.orggeochem.2010.07.001>
- Scott DT, Runkel RL, McKnight DM, Voelker BM, Kimball BA, Carraway ER (2003) Transport and cycling of iron and hydrogen peroxide in a freshwater stream: influence of organic acids. *Water Resour Res*. <https://doi.org/10.1029/2002WR001768>
- Senesi N, D'Orazio V (2005) Fluorescence spectroscopy. In: Hillel D (ed) *Encyclopedia of soils in the environment*, p 35–52. Oxford: Elsevier. <https://doi.org/10.1016/B0-12-348530-4/00211-3>
- Soong JL, Parton WJ, Calderon F, Campbell EE, Cotrufo MF (2015) A new conceptual model on the fate and controls of fresh and pyrolyzed plant litter decomposition. *Biogeochem* 124:27–44. <https://doi.org/10.1007/s10533-015-0079-2>
- Steele MK, Aitkenhead-Peterson JA (2013) Salt impacts on organic carbon and nitrogen leaching from senesced vegetation. *Biogeochem* 112:245–259. <https://doi.org/10.1007/s10533-012-9722-3>
- Stubbins A, Niggemann J, Dittmar T (2012) Photo-lability of deep ocean dissolved black carbon. *Biogeosciences* 9:1661–1670. <https://doi.org/10.5194/bg-9-1661-2012>
- Tuominen L, Kairesalo T, Hartikainen H (1994) Comparison of methods for inhibiting bacterial activity in sediment. *Appl Environ Microbiol* 60:3454–3457. <https://doi.org/10.1128/aem.60.9.3454-3457.1994>
- United States Geological Survey (USGS) (2018) “Water Quality after a Wildfire.” 6 Mar 2018. <https://ca.water.usgs.gov/wildfires/wildfires-water-quality.html>
- Uzun H, Dahlgren RA, Olivares C, Erdem CU, Karanfil T, Chow AT (2020) Two years of post-wildfire impacts on dissolved organic matter, nitrogen, and precursors of disinfection by-products in California stream waters. *Water Res* 181:115891. <https://doi.org/10.1016/j.watres.2020.115891>
- Wagner S, Jaffé R (2015) Effect of photodegradation on molecular size distribution and quality of dissolved black carbon. *Organic Geochem* 86:1–4. <https://doi.org/10.1016/j.orggeochem.2015.05.005>
- Wagner S, Cawley KM, Rosario-Ortiz FL, Jaffé R (2015) In-stream sources and links between particulate and dissolved black carbon following a wildfire. *Biogeochemistry* 124:145–161. <https://doi.org/10.1007/s10533-015-0088-1>
- Wagner S, Jaffé R, Stubbins A (2018) Dissolved black carbon in aquatic ecosystems. *Limnol Oceanogr Lett* 3:168–185. <https://doi.org/10.1002/lo2.10076>
- Wang J, Dahlgren RA, Erşan MS, Karanfil T, Chow AT (2015) Wildfire altering terrestrial precursors of disinfection byproducts in forest detritus. *Environ Sci Technol* 49:5921–5929. <https://doi.org/10.1021/es505836m>
- Wang H, Zhou H, Ma J, Nie J, Yan S, Song W (2020) Triplet photochemistry of dissolved black carbon and its effects on the photochemical formation of reactive oxygen species. *Environ Sci Technol* 54:4903–4911. <https://doi.org/10.1021/acs.est.0c00061>
- Ward CP, Cory RM (2016) Complete and partial photo-oxidation of dissolved organic matter draining permafrost soils. *Environ Sci Technol* 50:3545–3553. <https://doi.org/10.1021/acs.est.5b05354>
- Ward CP, Sleighter RL, Hatcher PG, Cory RM (2014) Insights into the complete and partial photooxidation of black carbon in surface waters. *Environ Sci Process Impacts* 16:721–731. <https://doi.org/10.1039/C3EM00597F>
- Wickland KP, Neff JC, Aiken GR (2007) Dissolved organic carbon in Alaskan boreal forest: sources, chemical characteristics, and biodegradability. *Ecosystems* 10:1323–1340. <https://doi.org/10.1007/s10021-007-9101-4>
- Wozniak AS, Goranov AI, Mitra S, Bostick KW, Zimmerman AR, Schlesinger DR, Myneni S, Hatcher PG (2020) Molecular heterogeneity in pyrogenic dissolved organic matter from a thermal series of oak and grass chars. *Organic Geochem* 148:104065. <https://doi.org/10.1016/j.orggeochem.2020.104065>
- Wymore AS, Compson ZG, McDowell WH, Potter JD, Hungate BA, Whitham TG, Marks JC (2015) Leaf-litter leachate is distinct in optical properties and bioavailability to stream heterotrophs. *Freshwater Sci* 34:857–866. <https://doi.org/10.1086/682000>
- Yan W, Chen Y, Han L, Sun K, Song F, Yang Y, Sun H (2022) Pyrogenic dissolved organic matter produced at higher temperature is more photoactive: insight into molecular changes and reactive oxygen species generation. *J Hazard Mater* 425:127817. <https://doi.org/10.1016/j.jhazmat.2021.127817>
- Zhang P, Huang P, Xu X, Sun H, Jiang B, Liao Y (2020) Spectroscopic and molecular characterization of biochar-derived dissolved organic matter and the associations with soil microbial responses. *Sci Total Environ* 708:134619. <https://doi.org/10.1016/j.scitotenv.2019.134619>